Scientific Reports

https://doi.org/10.1038/s41598-026-46657-w

Article in Press

ELF3 drives glioblastoma multiforme progression through the regulation of MXRA8 expression

Received: 17 March 2025

Accepted: 26 March 2026

Published online: 01 April 2026

Cite this article as: Wang M., Bo H., Chen D. *et al.* ELF3 drives glioblastoma multiforme progression through the regulation of MXRA8 expression. *Sci Rep* (2026). https://doi.org/10.1038/s41598-026-46657-w

Maomao Wang, Haiji Bo, Dapeng Chen, Jiangxin Mao, Zong Miao & Laixing Wang

ELF3 Drives Glioblastoma Multiforme Progression Through the Regulation of MXRA8 Expression

Maomao Wang[1#], Haiji Bo[2#], Dapeng Chen[3#], Jiangxin Mao[1], Zong Miao [1*], Laixing Wang [1*]

1. Department of Neurosurgery, Changhai Hospital of the Naval Medical University, Shanghai, 200434, China.

2. Department of Pathology, Naval Medical Center of PLA, No. 338 Huaihai West Road, Shanghai, 200052, China.

3. Department of Neurosurgery, Bozhou District People's Hospital of Zunyi City, Zunyi City, Guizhou Province, China, 563100.

[#]: These authors contribute equally to this study.

*: Corresponding authors: 1. Zong Miao, Department of Neurosurgery, Changhai Hospital of the Naval Medical University, Shanghai, 200434, China. Tel: (+86) 15300618451; Email: drmiaozong@126.com. 2. Laixing Wang, Department of Neurosurgery, Changhai Hospital of the Naval Medical University, Shanghai, 200434, China. Tel: (+86) 13918168327; Email: wlxsmmu@163.com.

Abstract

Background: Glioblastoma multiforme (GBM) is a highly aggressive brain tumor with limited treatment options and a poor prognosis. Its defining features include rapid proliferation, invasive capacity, and resistance to therapy. **Materials and Methods:** Bioinformatics analyses using TCGA and UALCAN datasets were conducted to assess MXRA8 and ELF3 expression and their association with patient survival. The expression levels were validated through qPCR and western blotting. Functional assays, including proliferation, migration, and invasion tests, were performed after silencing or overexpressing MXRA8 and ELF3. Chromatin immunoprecipitation (ChIP) and dual-luciferase reporter assays determined ELF3's role in regulating MXRA8 transcription. An *in vivo* xenograft model was used to evaluate the effects of ELF3 and MXRA8 on tumor growth. **Results:** MXRA8 expression was significantly elevated in GBM tissues and associated with reduced overall survival. Functional analyses revealed that MXRA8 knockdown inhibited oncogenic traits. Moreover, ELF3 was overexpressed in GBM tissues and positively correlated with MXRA8 expression. ChIP and dual-luciferase assays confirmed that ELF3 binds to the MXRA8 promoter and activates its transcription. Rescue experiments showed that MXRA8 overexpression could reverse the tumor-suppressive effects of ELF3 knockdown. *In vivo*, silencing ELF3 or MXRA8 inhibited tumor growth and proliferation. **Conclusion:** This study suggests that the ELF3-MXRA8 axis may be a critical driver of GBM progression, with ELF3 promoting tumor growth and invasion through transcriptional activation of MXRA8.

Keywords: Glioblastoma multiforme, ELF3, MXRA8, transcriptional regulation, tumor progression, therapeutic target

1 Introduction

Glioblastoma multiforme (GBM) is the most aggressive and prevalent malignant brain tumor in adults, accounting for approximately 48% of all central nervous system cancers[1]. Despite advancements in neurosurgery, radiotherapy, immunotherapy, and chemotherapeutic strategies such as temozolomide, the prognosis for patients with GBM remains grim, with a median survival of just 14–16 months[2, 3]. This poor outlook is attributed to the tumor's highly invasive nature, cellular heterogeneity, and resistance to conventional treatments[4, 5]. Although significant efforts have been made to uncover the molecular drivers of GBM with the goal of identifying new therapeutic targets[6, 7], the mechanisms underlying its progression and malignancy remain poorly understood[8]. This highlights the urgent need to identify novel regulators and pathways that may drive tumor progression and form the basis for new therapeutic strategies.

Matrix remodeling-associated 8 (MXRA8), a transmembrane protein involved in cell adhesion and extracellular matrix interactions[9], has gained attention as a receptor for several arthritogenic alphaviruses and a mediator of immune regulation[10-12]. Recent studies suggest that in GBM, MXRA8 plays a role in modulating ferroptosis and enhancing immune responses within tumor cells[11]. While evidence indicates that MXRA8 may influence cell invasion and migration in other cancer types[9, 12-15], its expression, functional significance, and prognostic value in GBM remain insufficiently explored. Investigating the potential role of MXRA8 in GBM progression could provide novel insights into its molecular mechanisms and offer novel therapeutic avenues.

Additionally, ELF3 (E74-like factor 3), a member of the ETS transcription factor family, has been implicated in regulating cell

proliferation, migration, and invasion across various cancers[16]. ELF3's role as either a tumor suppressor or oncogene is context-dependent, varying between cancer types[16]. In ovarian cancer, elevated ELF3 expression has been linked to increased cell proliferation and invasion, promoting disease progression[17, 18]. Conversely, in biliary tract and bladder cancers, reduced ELF3 expression correlates with weakened cell junctions and enhanced invasiveness[19, 20]. However, its precise molecular function in GBM remains inadequately defined. The potential of ELF3 to regulate downstream targets in driving tumor progression warrants further investigation.

This study investigates the role of the ELF3-MXRA8 axis in GBM progression. By employing bioinformatics analysis, *in vitro* functional assays, and *in vivo* xenograft models, the expression, regulation, and functional implications of MXRA8 and its transcriptional regulator ELF3 were explored. Our findings underscore the critical role of ELF3 in driving GBM progression through the activation of MXRA8, suggesting that targeting this axis may offer promising therapeutic strategies for GBM treatment.

2 Materials and Methods

2.1 Cell Culture and Reagents

The GBM cell lines U251, A172, and LN229, along with normal human astrocytes (NHA) cells, were obtained from Shanghai Zhongke-Huamei Biotechnology Co., Ltd. (Shanghai, China). Cells were cultured in Dulbecco's Modified Eagle Medium (DMEM) (Gibco, #11965092) supplemented with 10% fetal bovine serum (FBS) (Gibco, #10099-141) and 1% penicillin-streptomycin (Pen-Strep) (Gibco, #15140122), and incubated at 37°C in a humidified atmosphere with 5% CO_2. Cells were passaged at approximately 80%

confluency to maintain optimal growth conditions.

2.2 Bioinformatics Analysis

To assess MXRA8 and ELF3 expression in GBM, publicly available datasets from The Cancer Genome Atlas (TCGA) were retrieved and analyzed using the UALCAN database (https://ualcan.path.uab.edu/). The differential expression of MXRA8 was compared between normal brain tissues and primary GBM samples, further stratified by patient gender, TP53 mutation status, and age groups. Kaplan-Meier survival analysis was performed using TCGA data. Transcription factors potentially regulating MXRA8 were identified by integrating the JASPAR (for transcription factor prediction) and GEPIA (for GBM prognosis-associated genes) databases. Cross-referencing these datasets revealed three potential candidates: VDR, NKX3-1, and ELF3. The differential expression of these transcription factors in normal brain tissues and GBM samples was analyzed using TCGA data. Additionally, Pearson's correlation analysis was conducted to explore the relationship between MXRA8 and ELF3 mRNA expression. To validate the expression profile of MXRA8 in GBM across multiple platforms and to assess its specificity compared to other tumor types, we performed additional bioinformatic analyses as shown in Supplementary Figure S1. The GEPIA database (http://gepia.cancer-pku.cn/) was used to compare MXRA8 expression between GBM tissues (TCGA dataset) and normal brain tissues (GTEx dataset). Pan-cancer expression analysis of MXRA8 was conducted using GEPIA, which includes expression data from 31 cancer types in TCGA and paired normal tissues from GTEx. Expression levels of extracellular matrix-related genes (MMP2, MMP9, ITGB1) in GBM vs. normal brain tissues were also extracted from GEPIA for comparative purposes. Correlation analysis between

MXRA8 expression and established GBM molecular markers (EGFR, IDH1, MGMT) was performed using TCGA-GBM RNA-seq data in the GEPIA database.

2.3 Clinical sample collection

21 samples of GBM tissue and 13 samples of normal tissue were collected from the Department of Neurosurgery, Changhai Hospital of the Naval Medical University between January 2023 and December 2024. Patients gave informed consent and the research was approved and overseen by the Ethics Committee of Changhai Hospital (CHEC2023-153). The tissue samples were all snap-frozen and stored at − 80 °C. All GBM tissue samples were retrospectively reviewed and classified according to the WHO 2021 criteria. IDH mutation status was determined by immunohistochemistry for IDH1 R132H and/or next-generation sequencing. Only samples confirmed to be IDH-wildtype were included in the final analysis as “GBM”.

2.4 Quantitative PCR (qPCR)

Total RNA was extracted from cultured cells and tissue samples using the RNeasy Mini Kit (Qiagen, #74104). The integrity and purity of the RNA were confirmed *via* quantification with the NanoDrop spectrophotometer (Thermo Fisher Scientific, ND-2000). Complementary DNA (cDNA) synthesis was carried out using the PrimeScript RT Reagent Kit (Takara, #RR037A). Quantitative real-time PCR (qPCR) was performed on a StepOnePlus Real-Time PCR System (Applied Biosystems, #4376600) with SYBR Green PCR Master Mix (Applied Biosystems, #4309155). Specific primers for MXRA8 (forward: 5'-GCAACCTGCACCATCACTACT-3'; reverse: 5'-CCACCTGTTGAGCCTCCTC-3'), ELF3 (forward: 5'-TCTTCCCCAGCGATGGTTTTC-3'; reverse: 5'-

TCCCGGATGAACTCCCACA-3'), and the reference gene GAPDH (forward: 5'-ACAACTTTGGTATCGTGGAAGG-3'; reverse: 5'-GCCATCACGCCACAGTTTC-3') were synthesized by Sangon Biotech (Shanghai, China). Primer sequences were designed using Primer-BLAST (NCBI) to ensure specificity. Relative gene expression was quantified using the $2^{-\Delta\Delta Ct}$ method.

2.5 Western Blot Analysis

Cells and tissue samples were lysed using RIPA Lysis Buffer (Thermo Fisher Scientific, #89900) with a protease inhibitor cocktail (Roche, #04693124001) to prevent protein degradation. The lysates were incubated on ice for 30 minutes, vortexed intermittently to ensure complete lysis, and then centrifuged at 12,000 × g for 15 minutes at 4°C. The supernatants containing total protein were collected. Protein concentration was measured using the Pierce BCA Protein Assay Kit (Thermo Fisher Scientific, #23225). Equal protein amounts (20 µg) were separated by 10% SDS-PAGE and transferred to PVDF membranes (Millipore, #IPFL00010). Membranes were blocked with 5% non-fat milk in TBST (Tris-buffered saline with 0.1% Tween-20) for 1 hour at room temperature, then incubated overnight at 4°C with primary antibodies against MXRA8 (Abcam, #ab185444), ELF3 (Thermo Fisher Scientific, #ARC1191), and GAPDH (Proteintech, #60004-1-Ig, loading control). After washing, membranes were incubated with HRP-conjugated secondary antibodies (Cell Signaling Technology, #7074 for anti-rabbit or #7076 for anti-mouse) for 1 hour at room temperature. Protein bands were visualized using the ECL detection system (Thermo Fisher Scientific, #32106) and captured using a chemiluminescent imaging system.

2.6 Transfection and Plasmid Construction

Two distinct short hairpin RNAs (shRNAs) targeting MXRA8 (sh-MXRA8-1: forward oligo: 5'-CCGGACCTGCCACCATCACAATAAACTCGAGTTTATTGTGATGGTGGCAGGTTTTTTG-3'; reverse oligo: 5'-AATTCAAAAAACCTGCCACCATCACAATAAACTCGAGTTTATTGTGATGGTGGCAGGT-3'; sh-MXRA8-2: forward oligo: 5'-CCGGTGAGGACATCCAGCTAGATTACTCGAGTAATCTAGCTGGATGTCCTCATTTTTG-3'; reverse oligo: 5'-AATTCAAAAATGAGGACATCCAGCTAGATTACTCGAGTAATCTAGCTGGATGTCCTCA-3') and one short interfering RNA (siRNA) targeting ELF3 (si-ELF3: 5'-GGGTTTGAAGCTGACTTTATA-3') were designed and synthesized by GenePharma (Shanghai, China). A non-targeting negative control shRNA/siRNA (sh/si-NC) was used as a calibrator to ensure specificity of the knockdown. For rescue experiments, an MXRA8 overexpressing plasmid (pcDNA3.1-MXRA8) and an empty vector (pcDNA3.1) were obtained from GeneCopoeia (Rockville, MD, USA). The plasmid encoding MXRA8 was designed to restore MXRA8 expression in cells where ELF3 had been silenced, enabling the evaluation of ELF3's functional dependence on MXRA8 in promoting GBM malignancy.

Transfections of shRNAs/siRNAs or plasmids into U251 and LN229 GBM cells were carried out using Lipofectamine 3000 (Thermo Fisher Scientific, #L3000015). Cells were seeded at a density of 2×10^5 cells per well in 6-well plates and cultured to approximately 60–70% confluency. Lipofectamine 3000 was used to complex the shRNA/siRNA or plasmid with the transfection reagent in a serum-free medium, which was then added to the cells. After a 6-hour incubation, the medium was replaced with a complete medium. Cells were harvested 48 hours post-transfection for

downstream assays, including protein and RNA extraction, cell viability assays, and functional analyses.

2.7 Cell Proliferation, Viability, and Colony Formation Assays

Cell viability was assessed using the CCK-8 assay (Cell Counting Kit-8, Dojindo, #CK04). Cells were harvested, resuspended in a complete growth medium, and seeded at a density of 5×10^3 cells per well into 96-well plates, with triplicates for each condition. After incubation for 24, 48, and 72 hours, 10 µL of CCK-8 reagent was added to each well, followed by an additional 2-hour incubation at 37°C. The metabolic activity and viability were quantified by measuring absorbance at 450 nm using a SpectraMax i3x plate reader (Molecular Devices, #SMAX3). To ensure consistency, the assay was performed in triplicate on separate occasions.

For colony formation assays, the long-term proliferative capacity of cells was evaluated. Stable U251 cell lines were generated using lentiviral systems. Lentiviruses were added to U251 cells at an MOI of 10 (optimized in preliminary experiments) in the presence of 8 µg/mL polybrene. To generate MXRA8-overexpressing (OE) stable U251 cells, the full-length human MXRA8 cDNA was cloned into the lentiviral expression vector pLVX-Puro (Clontech). To generate ELF3-knockdown stable cells, a specific short hairpin RNA (shRNA) sequences targeting ELF3 were cloned into the pLKO.1-puro lentiviral vector (Addgene). A non-targeting shRNA (sh-NC) was used as control. Lentiviruses were produced by co-transfecting the constructed vectors with packaging plasmids (psPAX2 and pMD2.G) into HEK293T cells using Lipofectamine 3000. Viral supernatants were collected at 48 and 72 hours post-transfection, filtered, and concentrated. Target GBM cells (U251) were infected with the lentiviruses in the presence of 8 µg/mL polybrene. After 24 hours,

the medium was replaced with fresh complete medium. Forty-eight hours post-infection, U251 cells were selected with 2 μg/mL puromycin for 7 days to obtain stable polyclonal populations. The knockdown efficiency of ELF3 and the overexpression level of MXRA8 were confirmed by Western blot analysis before subsequent functional assays (Supplemental Figure S2). A total of 500 cells per well were plated in 6-well plates in triplicate and allowed to grow undisturbed for 10 days. Colonies were fixed with 4% paraformaldehyde (Sigma-Aldrich, #P6148), stained with 0.1% crystal violet (Sigma-Aldrich, #C0775), and excess dye was washed off with distilled water. The plates were dried in an air-conditioned environment, and colonies were counted manually using a light microscope. The average colony count per well was calculated and compared across experimental groups to assess the impact of gene manipulation on cellular proliferation.

2.8 Transwell Invasion and Migration Assays

Cell invasion and migration were assessed using Transwell inserts (Corning, #3422) with 8-μm pores. The inserts were either coated with Matrigel (Corning, #354234) to evaluate invasive capacity or left uncoated for migration analysis. Matrigel was thawed overnight on ice, diluted in serum-free DMEM to the recommended concentration, and 100 μL of the diluted Matrigel was applied to the upper chamber membrane, allowing it to solidify at 37°C for 30 minutes prior to the invasion assay.

For both assays, cells were collected, resuspended in serum-free DMEM, and adjusted to a concentration of 2×10^4 cells per well. A total of 200 μL of the prepared cell suspension was introduced into the upper chamber, while the lower chamber contained 600 μL of DMEM supplemented with 10% FBS. The plates were incubated at

37°C in a humidified environment for 24 hours, allowing cells to either migrate through the uncoated membrane or invade through the Matrigel barrier toward the chemoattractant.

After incubation, non-migratory or non-invasive cells remaining on the upper membrane were removed using a cotton swab. Cells that migrated or invaded to the lower membrane were fixed with 4% paraformaldehyde and stained with 0.1% crystal violet (Sigma-Aldrich, #C0775). Excess stain was washed off with distilled water, and the membranes were air-dried. Stained cells were visualized using a light microscope, with five random fields per chamber (200 × magnification) analyzed. The average number of migrated or invaded cells per group was determined, and all experiments were performed in triplicate to ensure reproducibility.

2.9 Wound Healing Assay

Cells were cultured in 6-well plates to 90–95% confluence. A sterile 200-µL pipette tip was used to create a uniform linear scratch (wound) across the cell monolayer. Detached cells and debris were removed by washing twice with phosphate-buffered saline (PBS, Gibco, #10010023). The cells were then cultured in serum-free DMEM to minimize proliferation and focus on migration. Immediately after scratching (time 0 h), images of the wound were captured using an inverted microscope (Olympus IX73) at 100 × magnification. Plates were incubated at 37°C, and wound closure was monitored at 24 hours. At this time, images of the same wound areas were captured. Wound closure was analyzed using ImageJ software, quantifying the wound area at each time point and calculating the percentage of closure.

2.10 EdU Proliferation Assay

Cells were seeded into 24-well plates at a density of 5×10^4 cells per well. The EdU labeling reagent (BeyoClick EdU Cell Proliferation Kit with Alexa Fluor 594, Beyotime, #C0078S) was added to the culture medium, and cells were incubated for 2 hours at 37°C in a 5% CO_2 atmosphere. After incubation, the cells were washed with PBS, fixed in 4% paraformaldehyde for 15 minutes, and permeabilized with 0.5% Triton X-100 (Sigma-Aldrich, #T8787) in PBS for 10 minutes. Cells were then incubated with Alexa Fluor 594 fluorescent dye for 30 minutes in the dark at room temperature. Nuclei were counterstained with DAPI (Beyotime, #C1005) for 10 minutes. Images of EdU-positive (red) and total nuclei (blue) were captured using a Leica DMi8 fluorescence microscope at 200 × magnification. The percentage of proliferating cells was calculated by determining the ratio of EdU-positive nuclei to total nuclei in five randomly selected fields per well.

2.11 Chromatin Immunoprecipitation (ChIP) Assay

ELF3 binding to the MXRA8 promoter was evaluated using a chromatin immunoprecipitation (ChIP) assay (ChIP Assay Kit, Abcam, #ab500). U251 and LN229 glioblastoma cells were cultured to 80–90% confluence and then treated with 1% formaldehyde (Sigma-Aldrich, #F8775) to crosslink proteins to DNA. Crosslinking was terminated by adding 125 mM glycine, and the cells were washed twice with ice-cold PBS to remove any residual crosslinkers. The cells were then lysed using the provided lysis buffer, and chromatin was sheared into DNA fragments ranging from 200 to 500 bp using a Bioruptor Pico (Diagenode, #B01060001). Fragmentation efficiency was confirmed by agarose gel electrophoresis. For immunoprecipitation, sheared chromatin was incubated overnight at 4°C with an anti-ELF3 antibody (Thermo Fisher Scientific,

#ARC1191) or normal IgG (negative control). Protein A/G magnetic beads were then added to isolate the antibody-protein-DNA complexes. After extensive washing, the crosslinking was reversed by heating at 65°C, and the immunoprecipitated DNA was purified using spin columns from the kit. The enriched DNA was analyzed by PCR using primers targeting potential ELF3-binding sites in the MXRA8 promoter. The PCR products were visualized *via* agarose gel electrophoresis.

2.12 Dual-Luciferase Reporter Assay

The MXRA8 wild-type promoter construct (MXRA8-WT) and the mutant construct lacking the ELF3-binding site (MXRA8-MT) were synthesized by GenePharma (Shanghai, China) and cloned into the pGL3-Basic luciferase vector (Promega, #E1751) upstream of the firefly luciferase gene. For the luciferase assay, U251 and LN229 glioblastoma cells were seeded in 24-well plates at 1×10^5 cells per well and allowed to adhere overnight. The cells were then co-transfected with either MXRA8-WT or MXRA8-MT constructs (200 ng) along with a Renilla luciferase plasmid (50 ng, internal control; Promega, #E2231) using Lipofectamine 3000. To investigate the role of ELF3, cells were also co-transfected with either si-ELF3 or si-NC (50 nM). After 48 hours, luciferase activity was measured using the Dual-Luciferase Reporter Assay System (Promega, #E1910). Cells were lysed with 100 µL of passive lysis buffer, and 20 µL of lysate was transferred to a 96-well plate. Firefly and Renilla luciferase activities were sequentially measured with a luminometer (SpectraMax i3x, Molecular Devices). The relative luciferase activity was calculated as the ratio of firefly to Renilla signals, then normalized to the si-NC control group.

2.13 Gene Knockout

Single-guide RNAs (sgRNAs) targeting ELF3 and MXRA8 were designed using the online CRISPR tool (http://crispr.mit.edu) and synthesized by GenePharma (Shanghai, China). The sgRNA sequences were cloned into the lentiCRISPR v2 plasmid (Addgene, #52961). Lentivirus production was achieved by co-transfecting HEK293T cells with the lentiCRISPR v2 plasmid, psPAX2 packaging plasmid (Addgene, #12260), and pMD2.G envelope plasmid (Addgene, #12259), facilitated by Lipofectamine 3000. Lentiviral supernatants were collected 48 hours post-transfection, filtered through a 0.45-μm filter, and concentrated using Lenti-X Concentrator (Takara, #631231). U251 glioblastoma cells were transduced with lentivirus carrying ELF3-KO, MXRA8-KO, or Cas9-NC sgRNAs in the presence of 8 μg/mL polybrene (Sigma-Aldrich, #H9268). Successfully transduced cells were selected with 2 μg/mL puromycin (Sigma-Aldrich, #P8833) for 7 days. Gene knockout efficiency was validated by Western blotting.

2.14 *In Vivo* Xenograft Studies

Four-week-old male BALB/c nude mice were obtained from Beijing Vital River Laboratory Animal Technology (Beijing, China). U251 glioblastoma cells transduced with ELF3-KO, MXRA8-KO, or Cas9-NC constructs were harvested during the logarithmic growth phase. The cells were washed twice with sterile PBS, resuspended at 5×10^6 cells per 100 μL of PBS, and then injected subcutaneously into the right flank of each mouse using a 27-gauge needle. Five mice were randomly included in each experimental group. Tumor growth was monitored by measuring tumor length and width every 5 days with digital calipers, and tumor volume was calculated using the formula $(\text{length} \times \text{width}^2)/2$. Throughout the 35-day experiment, the

mice were closely observed for weight changes, general health, and signs of distress to ensure humane treatment. At the study's conclusion, mice were euthanized by quick cervical dislocation method and the tumors were excised, weighed, and photographed for further analysis. All methods were carried out in accordance with relevant guidelines and regulations. The animal study was also approved by the Ethics Committee of Shanghai Changhai Hospital (CHEC2024-105).

2.15 Immunohistochemistry (IHC)

Tumor tissues were carefully excised at the end of the experiment and immediately fixed in 4% paraformaldehyde at room temperature for 24 hours to preserve tissue morphology and antigenicity. The fixed tissues were then processed through ethanol gradients for dehydration, cleared in xylene, and embedded in paraffin to form tissue blocks. These blocks were sectioned into 5-μm slices using a microtome (Leica RM2235) and mounted onto glass slides. For IHC, the slides were deparaffinized with xylene, rehydrated through a descending ethanol series, and rinsed in distilled water. Antigen retrieval was performed by heating the slides in citrate buffer at 95°C for 15 minutes using a microwave, followed by cooling to room temperature. The sections were then blocked with 5% goat serum (Beyotime, #C0265) for 1 hour to minimize nonspecific binding. The following day, the slides were incubated overnight at 4°C with primary antibodies: anti-MXRA8 (Abcam, #ab185444, diluted 1:200) or anti-Ki-67 (Cell Signaling Technology, #9027, diluted 1:400). On the next day, sections were incubated with HRP-conjugated secondary antibodies (Abcam, #ab6721), and the signals were visualized using the DAB Substrate Kit (Abcam, #ab64238). After counterstaining with hematoxylin,

slides were rinsed and mounted with coverslips. Images were captured using a Nikon Eclipse microscope at 200 × magnification. Protein expression levels were quantified by assessing staining intensity and positive cell counts using ImageJ software.

2.16 Statistical Analysis

Data were processed and statistically analyzed using GraphPad Prism 8.0 (GraphPad Software, San Diego, CA, USA). Results are presented as mean ± standard deviation (SD). All quantitative data presented as mean ± standard deviation (SD) are derived from at least three independent biological replicates ($n \geq 3$), unless otherwise specified. A two-tailed Student's t-test was applied to assess differences between two groups. All experiments were conducted in triplicate, ensuring the reliability and reproducibility of the data. Statistical significance was defined as $P < 0.05$.

3 Results

3.1 MXRA8 Expression Enhanced in GBM with a Concomitant Correlation to Adverse Prognosis

To elucidate the expression pattern of MXRA8 in GBM, an in silico analysis was performed using TCGA datasets *via* the UALCAN database. The results revealed a significant increase in MXRA8 expression in primary GBM tumors compared to normal brain tissues (Figure 1A). Further stratification based on clinical characteristics confirmed consistent upregulation of MXRA8 across different patient gender (Figure 1B), TP53 mutation status (Figure 1C), and age groups (Figure 1D). Survival analysis indicated that higher MXRA8 expression was associated with a significant reduction in overall survival, compared to low expression levels (Figure 1E, Logrank $P = 0.012$, $HR = 1.6$). To validate these observations, 34

clinical samples, including 13 normal brain tissues and 21 GBM tissues, were analyzed. Consistent with the bioinformatics data, qPCR confirmed elevated MXRA8 expression in GBM tissues (Figure 1F). These results suggest that MXRA8 plays a pivotal role in GBM progression and may serve as a potential biomarker and therapeutic target. To further validate the specificity of MXRA8 upregulation in GBM, we performed cross-database analyses using GEPIA and GTEx. Consistent with TCGA data, MXRA8 expression was significantly elevated in GBM compared to normal brain tissues (Supplementary Fig. S1A). Pan-cancer analysis revealed that MXRA8 expression varies across tumor types, with particularly high levels in GBM, highlighting its potential tumor-type specificity (Supplementary Fig. S1B). Furthermore, comparison with other extracellular matrix-related genes (MMP2, MMP9, ITGB1) showed that these genes were also upregulated in GBM, suggesting a coordinated remodeling of the tumor microenvironment (Supplementary Fig. S1C). Correlation analysis with established GBM markers (EGFR, IDH1, MGMT) indicated that MXRA8 expression was significantly associated with MGMT but not significantly associated with EGFR or IDH1, implying a potential link to treatment response mechanisms (Supplementary Fig. S1D).

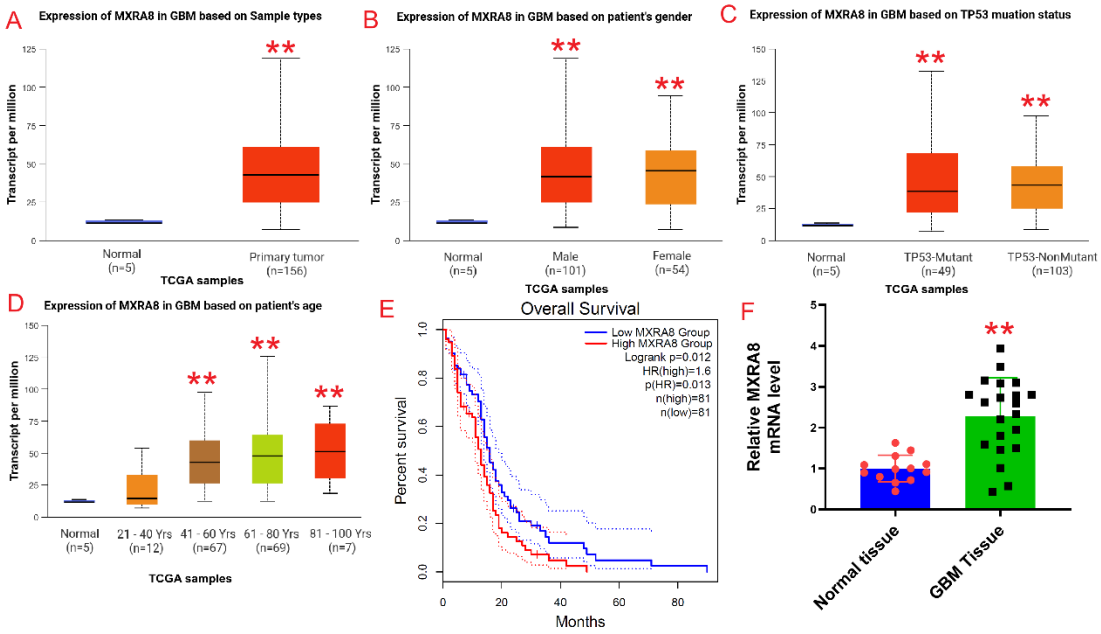

Figure 1. MXRA8 Expression is Elevated in GBM and Correlates with Poor Prognosis. (A) Boxplot showing significantly higher MXRA8 expression in primary GBM tumors, based on TCGA data. (B) Analysis of MXRA8 expression in GBM and normal tissues by patient gender, showing consistent upregulation in GBM. (C) Examination of MXRA8 expression in relation to TP53 mutation status, with both TP53-mutant and non-mutant GBM tissues showing elevated levels. (D) MXRA8 expression in GBM across different age groups, demonstrating consistent upregulation. (E) Kaplan-Meier survival curve showing reduced overall survival in patients with high MXRA8 expression. (F) qPCR analysis of MXRA8 mRNA levels in 13 normal brain tissues and 21 GBM tissues, showing significantly higher expression in GBM tissues.

3.2 ELF3 Is Highly Expressed in GBM and Correlates Positively with MXRA8 Expression and Poor Prognosis

To identify potential transcription factors (TFs) that regulate MXRA8 in GBM, data from the JASPAR and GEPIA databases were analyzed. Among 501 potential TFs for MXRA8 and 189 genes associated with GBM prognosis, three overlapping candidates were identified: VDR,

NKX3-1, and ELF3 (Figure 2A). Of these, only ELF3 exhibited significantly elevated expression in GBM tissues (Figure 2D), while VDR and NKX3-1 showed no notable changes (Figures 2B, 2C). Further analysis *via* the UALCAN database confirmed consistent upregulation of ELF3 expression across patient gender (Figure 2E), TP53 mutation status (Figure 2F), and age groups (Figure 2G). Patients were stratified into high and low ELF3 expression groups based on the median expression level in the TCGA-GBM cohort. Kaplan-Meier survival analysis revealed that patients with high ELF3 expression had poorer overall survival (Figure 2H). Validation with 34 clinical specimens, including 13 normal and 21 GBM tissues, confirmed elevated ELF3 mRNA levels in GBM tissues (Figure 2I). Additionally, a strong positive correlation was found between ELF3 and MXRA8 mRNA levels in GBM tissues (Figure 2J). These results suggest that ELF3 is a critical transcriptional regulator of MXRA8, contributing to GBM progression and poor prognosis. The results presented are limited to screening and correlation analyses; definitive evidence for a regulatory relationship was validated by subsequent ChIP and dual-luciferase reporter assays.

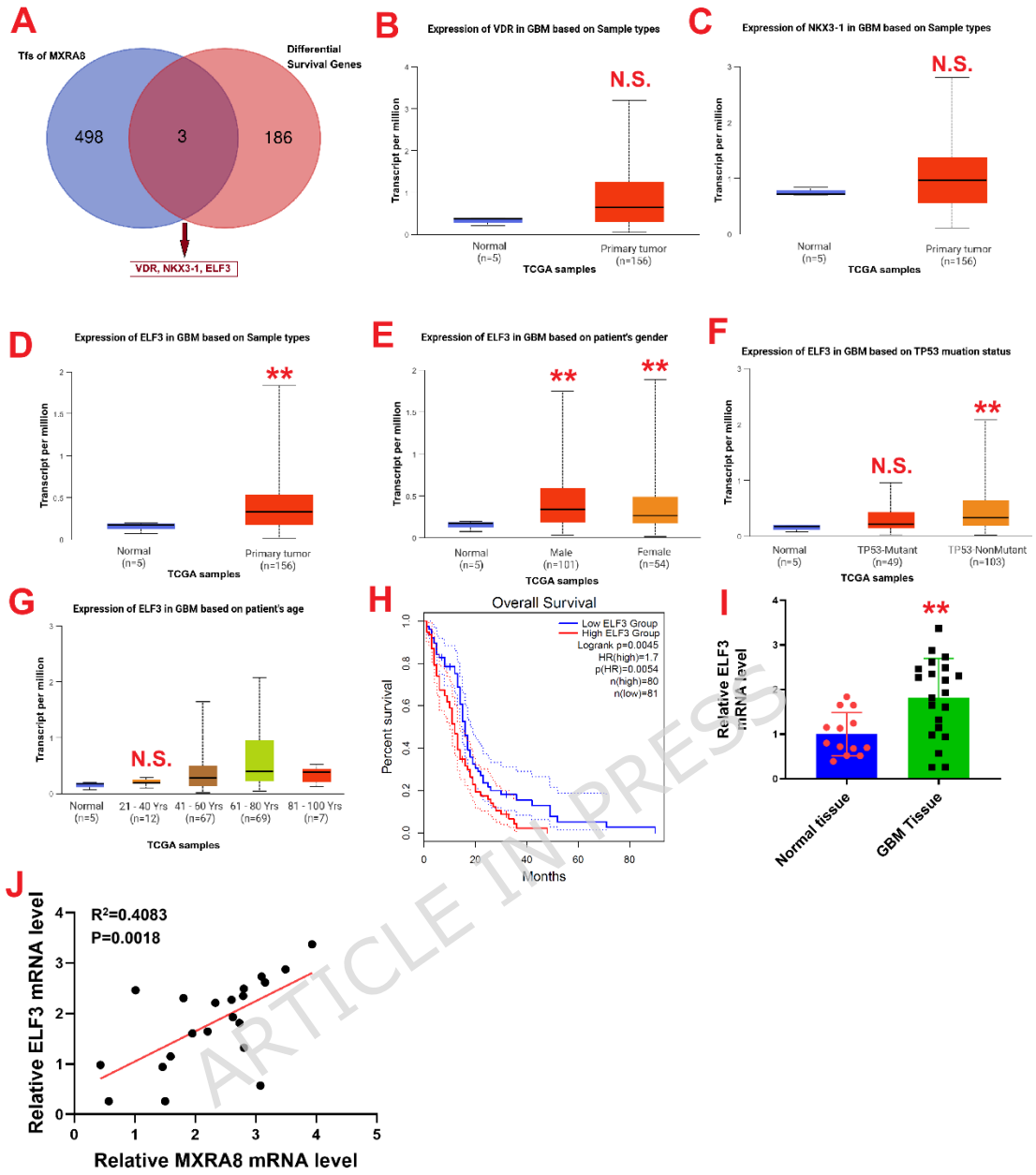

Figure 2. ELF3 Is Highly Expressed in GBM and Correlates with MXRA8 and Poor Prognosis. (A) Venn diagram showing the overlap of MXRA8 TFs predicted by JASPAR and GBM prognosis-related genes from GEPIA, identifying three candidates: VDR, NKX3-1, and ELF3. (B-C) Boxplots showing no significant difference in VDR (B) and NKX3-1 (C) expression between normal and GBM tissues. (D) Significant upregulation of ELF3 in GBM tissues. (E) ELF3 expression by patient gender, demonstrating consistent elevation in GBM tissues. (F) ELF3 expression significantly higher in TP53-

mutant and non-mutant GBM tissues. (G) ELF3 expression shows a trend toward upregulation in GBM tissues across age groups. (H) Kaplan-Meier survival curve showing reduced overall survival in patients with high ELF3 expression (Logrank P = 0.001, HR = 1.7). (I) qPCR confirming elevated ELF3 mRNA in GBM tissues compared to normal brain tissues ($P < 0.01$). (J) Positive correlation between ELF3 and MXRA8 mRNA levels in GBM tissues ($R^2 = 0.4083$, $P = 0.0018$).

3.3 MXRA8 Overexpression Promoted GBM Cell Viability and Proliferation

To investigate the functional role of MXRA8 in GBM, its expression was assessed in GBM cell lines (A172, U251, and LN229). Both qPCR and western blot analyses revealed significantly elevated MXRA8 expression at the transcription and protein levels in GBM cells compared to normal human astrocytes (NHA) (Figures 3A-B). To further explore its biological impact, MXRA8 expression was knocked down using two specific short hairpin RNAs (sh-MXRA8-1 and sh-MXRA8-2) in U251 and LN229 cells. Knockdown efficiency was confirmed by qPCR and western blot (Figures 3C-E). Functional assays revealed that MXRA8 knockdown significantly reduced cell viability in both U251 and LN229 cells over a 72-hour period (Figures 3F-G). Additionally, colony formation assays showed a marked reduction in colony numbers, indicating impaired proliferative capacity (Figures 3H-I). These results collectively demonstrate that MXRA8 is overexpressed in GBM cells and plays a critical role in promoting cell viability and proliferation.

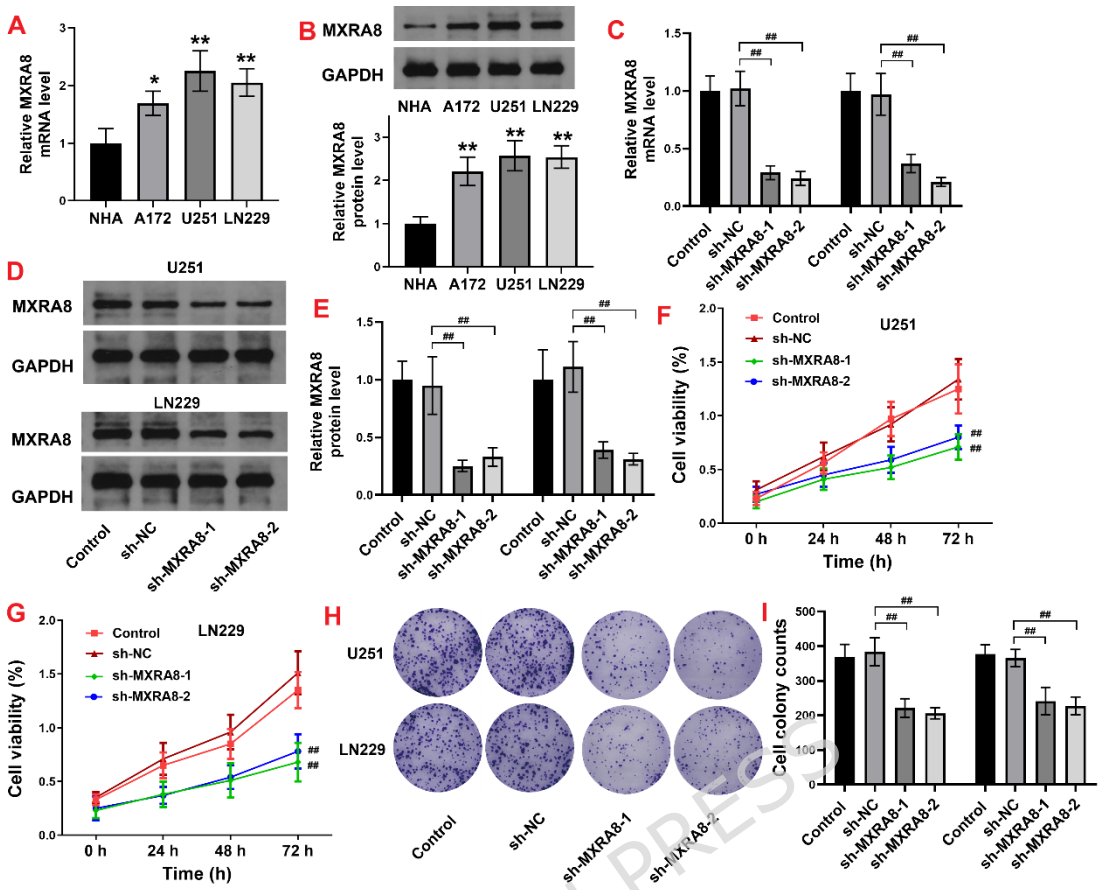

Figure 3. MXRA8 Overexpression Enhances GBM Cell Viability and Proliferation. (A) qPCR analysis showing elevated MXRA8 mRNA levels in A172, U251, and LN229 cell lines compared to NHA cells. (B) Western blot confirming increased MXRA8 protein expression in GBM cell lines. (C-E) Validation of MXRA8 knockdown efficiency in U251 and LN229 cells by qPCR (C) and western blot (D-E). (F-G) CCK-8 assay indicating reduced cell viability in U251 (F) and LN229 (G) cells after MXRA8 knockdown over 72 hours. (H-I) Colony formation assay showing a significant reduction in colony numbers following MXRA8 knockdown in U251 and LN229 cells. Gels/blots were cropped from different parts of the same gel. Data are presented as mean ± SD from three independent experiments.

3.4 MXRA8 Knockdown Suppressed GBM Cell Invasion, Migration, and Proliferation

To further elucidate the role of MXRA8 in GBM progression, its impact on various cellular behaviors was assessed in U251 and LN229 cells. Transwell invasion and migration assays demonstrated that MXRA8 knockdown significantly inhibited the invasive (Figures 4A, 4E) and migratory (Figures 4B, 4F) abilities of both cell lines, as indicated by a notable reduction in the number of invading and migrating cells. The wound healing assay reinforced these results, showing that MXRA8 knockdown impaired the wound closure capacity of GBM cells, suggesting compromised migratory ability (Figures 4C, 4G). Additionally, the EdU incorporation assay revealed a significant decrease in the proportion of proliferative, EdU-positive cells after MXRA8 silencing (Figures 4D, H). These results collectively indicate that MXRA8 is critical for maintaining the invasive, migratory, and proliferative phenotypes of GBM cells, underscoring its role in promoting aggressive tumor behavior.

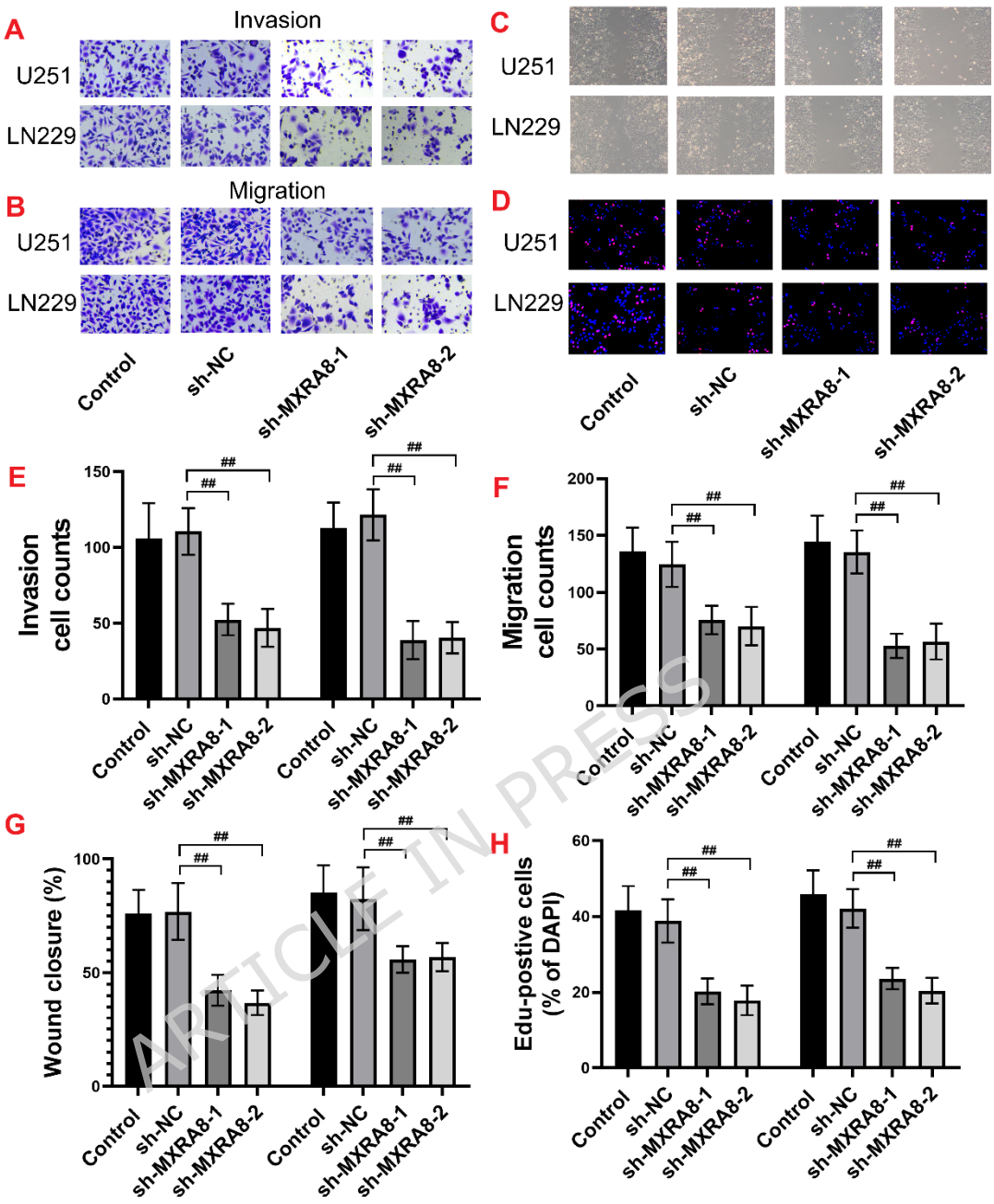

Figure 4. MXRA8 Knockdown Impairs GBM Cell Invasion, Migration, and Proliferation. (A-B) Representative images from Transwell assays showing reduced invasion (A) and migration (B) of U251 and LN229 cells after MXRA8 knockdown. (C) Wound healing assay showing impaired wound closure in U251 and LN229 cells with MXRA8 silencing. (D) EdU incorporation assay illustrating reduced percentages of proliferative, EdU-positive cells upon MXRA8 knockdown. (E-F) Quantification of invasive (E) and migratory (F)

cell counts in U251 and LN229 cells. (G) Quantification of wound closure percentage from the wound healing assay. (H) Quantification of EdU-positive cells as a percentage of DAPI-stained nuclei.

3.5 ELF3 Directly Activated MXRA8 Transcription *via* Promoter Binding

The molecular mechanism by which ELF3 regulates MXRA8 expression was explored by identifying three potential ELF3-binding sites within the MXRA8 promoter region (Site 1: 167-175, Site 2: 1302-1310, Site 3: 1339-1347) (Figure 5A). Chromatin immunoprecipitation (ChIP) assays showed significant ELF3 binding at Site 2 in both U251 and LN229 cells, with no enrichment at Sites 1 and 3 (Figures 5B-C). Dual-luciferase reporter assays further confirmed that ELF3 knockdown, validated by Western blot (Figure 5D), reduced luciferase activity in the wild-type MXRA8 promoter (MXRA8-WT) but not in a mutant promoter lacking Site 2 (MXRA8-MT) (Figures 5E-F). As expected, ELF3 knockdown significantly reduced the luciferase activity driven by the wild-type MXRA8 promoter (MXRA8-WT) in both cell lines (Figures 5E, F). In contrast, the mutant promoter lacking Site 2 (MXRA8-MT) exhibited markedly lower basal activity, and importantly, this residual activity was not further suppressed upon ELF3 knockdown. This indicates that the transcriptional activation of MXRA8 by ELF3 is predominantly mediated through its binding to Site 2. Correspondingly, ELF3 knockdown led to a significant decrease in both MXRA8 protein (Figures 5G-H) and mRNA levels (Figure 5I). Overall, the findings indicate that ELF3 directly binds to the MXRA8 promoter at Site 2 (1302-1310) and transcriptionally activates its expression, playing a pivotal role in MXRA8-mediated GBM progression.

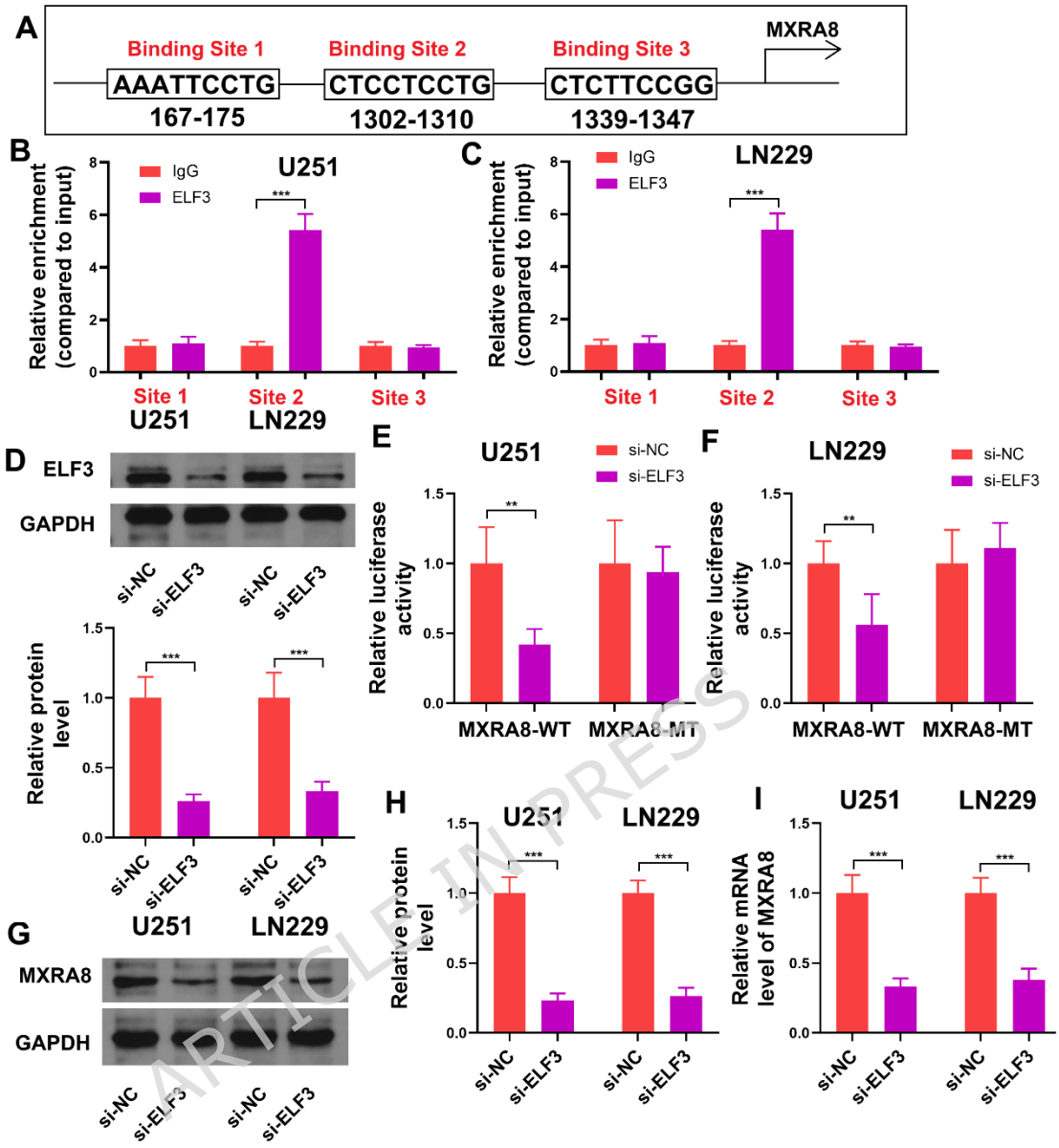

Figure 5. ELF3 Directly Activates MXRA8 Transcription *via* Promoter Binding. (A) Diagram of the three potential ELF3-binding sites in the MXRA8 promoter. (B-C) ChIP assays revealed significant ELF3 enrichment at Site 2 in U251 (B) and LN229 (C) cells. (D) Western blot confirmed efficient ELF3 knockdown in U251 and LN229 cells. (E-F) Dual-luciferase reporter assays showed reduced luciferase activity in U251 (E) and LN229 (F) cells with ELF3 knockdown at MXRA8-WT, but not at MXRA8-MT. The mutant promoter (MXRA8-MT) shows low basal activity which is not responsive to ELF3 knockdown, confirming Site 2 as the critical

functional binding site. (G-I) Western blot (G, H) and qPCR (I) analyses showed reduced MXRA8 protein and mRNA levels following ELF3 silencing. Gels/blots were cropped from different parts of the same gel. Data are presented as mean ± SD from three independent experiments.

3.6 MXRA8 Overexpression Countered the Tumor-Suppressive Effects of ELF3 Knockdown

The hypothesis that ELF3 promotes GBM progression through MXRA8 was tested *via* a series of rescue experiments. Functional assays demonstrated that stable ELF3 knockdown (shRNA) led to a marked decline in colony formation (Figures 6A-B). Short-term ELF3 knockdown (siRNA) resulted in a significant reduction in MXRA8 protein expression, which was restored by co-transfection with an MXRA8 overexpression plasmid (Figures 6C-D). Functional assays demonstrated that stable ELF3 knockdown significantly decreased cell proliferation (as measured by EdU staining, Figures 6E-F), and cell viability in a time-dependent manner (Figure 6G). Notably, MXRA8 overexpression reversed these inhibitory effects, restoring colony counts, EdU-positive cell numbers, and cell viability to levels comparable to the control group. Similarly, ELF3 knockdown impaired cell invasion and migration (Figures 6H-I), but these effects were also rescued by MXRA8 overexpression, highlighting the functional dependence of ELF3 on MXRA8 in driving GBM malignancy. Thus, our findings confirm that ELF3 exerts its pro-tumorigenic effects in GBM through the regulation of MXRA8, establishing the ELF3-MXRA8 axis as a critical pathway in GBM progression.

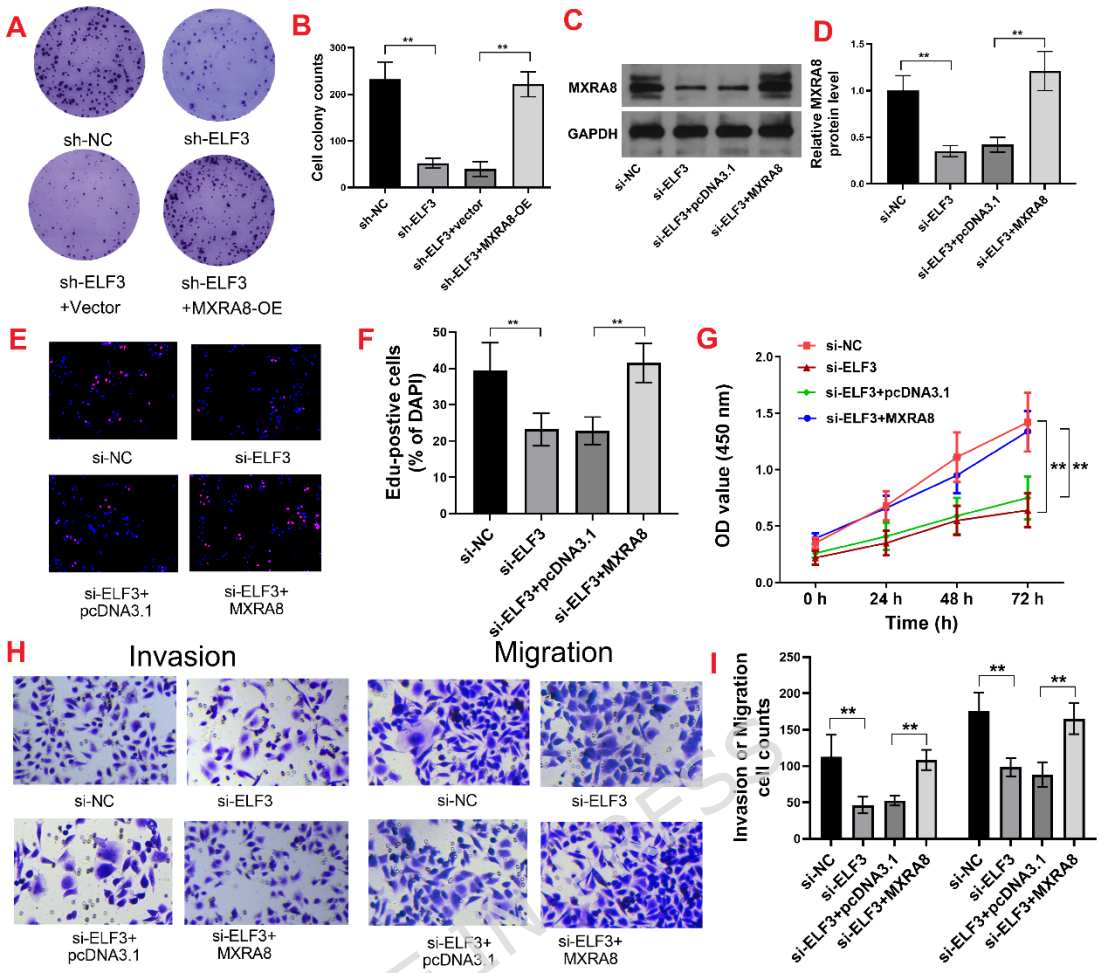

Figure 6. MXRA8 Overexpression Counteracts the Tumor-Suppressive Effects of ELF3 Knockdown. (A-B) Colony formation assay demonstrating reduced colony numbers after ELF3 knockdown (shRNA), reversed by MXRA8 overexpression (OE). (C-D) Western blot showing reduced MXRA8 protein levels following ELF3 knockdown, restored by MXRA8 overexpression. (E-F) EdU incorporation assay revealing diminished cell proliferation following ELF3 knockdown, rescued by MXRA8 expression. (G) CCK-8 assay showing a time-dependent reduction in cell viability with ELF3 silencing, restored by MXRA8 expression. (H-I) Transwell invasion and migration assays displaying impaired cell invasion and migration following ELF3 knockdown, reversed by MXRA8 expression. Gels/blots were cropped from different parts of the same gel. Data are presented as mean ± SD from three independent experiments.

3.7 ELF3 and MXRA8 Knockout (KO) Suppressed Tumor Growth *in Vivo*

To evaluate the roles of ELF3 and MXRA8 in GBM tumorigenesis *in vivo*, a xenograft model was established by implanting U251 cells into nude mice. Western blot analysis of the resulting tumors confirmed that knockout of ELF3 or MXRA8 significantly reduced MXRA8 protein levels (Figure 7A). Tumor growth was markedly inhibited in mice injected with ELF3- or MXRA8-silenced cells, evidenced by a significant reduction in both tumor volume (Figure 7B) and weight (Figure 7D) at the end of the 35-day experiment. Representative tumor images further demonstrated smaller tumors in the knockout groups (Figure 7E). Importantly, there were no significant changes in mouse body weight among the groups, indicating no obvious acute systemic toxicity associated with gene silencing (Figure 7C). Immunohistochemical analysis revealed a significant decrease in both MXRA8 and Ki-67 expression in the ELF3- or MXRA8-knockout tumors (Figure 7F), indicating reduced tumor cell proliferation. These results suggest that ELF3 and MXRA8 contribute to GBM tumor growth by promoting cell proliferation, and their silencing impedes tumor progression. In conclusion, this *in vivo* study highlights the critical role of the ELF3-MXRA8 axis in GBM and its potential as a therapeutic target for tumor suppression.

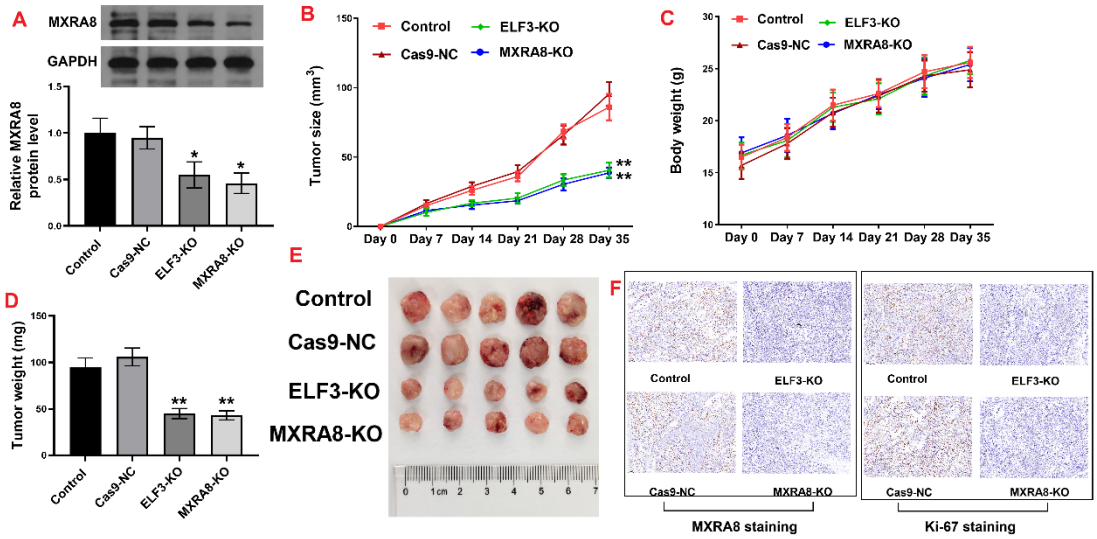

Figure 7. ELF3 and MXRA8 Knockout Suppresses Tumor Growth in a Xenograft Model. (A) Western blot analysis showing reduced MXRA8 protein levels in xenograft tumors after ELF3 or MXRA8 knockout (KO). (B) Tumor volume significantly decreased in the ELF3- or MXRA8-silenced groups. (C) No significant changes in mouse body weight, indicating no systemic toxicity. (D) A notable reduction in final tumor weight was observed on day 35 in the ELF3 and MXRA8 knockout groups. (E) Representative images showing smaller tumors in the knockout groups. (F) Immunohistochemical staining revealed decreased MXRA8 and Ki-67 expression in tumors with ELF3 or MXRA8 silencing. Gels/blots were cropped from different parts of the same gel. Data are presented as mean ± SD from three independent experiments.

4 Discussion

GBM is characterized by aggressive behavior and poor prognosis[1, 2]. Despite notable progress in surgical intervention, radiotherapy, and chemotherapy, these treatments yield only marginal improvements in patient survival, highlighting the urgent need for novel therapeutic approaches and a deeper understanding

of its molecular mechanisms[6-8].

This study demonstrates a significant overexpression of MXRA8, a transmembrane protein, in both GBM tissues and cell lines. A strong correlation exists between elevated MXRA8 levels and poor prognosis, suggesting its potential as both a biomarker and a driver of GBM malignancy. Notably, our bioinformatics analyses demonstrated that the high expression of MXRA8 and ELF3 in GBM was consistent across different subgroups stratified by sex, age, and TP53 mutation status (Figures 1 and 2). This pan-subgroup high-expression pattern suggests two key implications. From a biological perspective, the ELF3-MXRA8 axis may represent a relatively universal oncogenic mechanism that is not strongly dependent on the major patient subgroups defined by sex, age, or TP53 status. Its upstream regulatory mechanisms are likely positioned in the common signaling pathways downstream of these factors. In clinical translational perspective, this widespread high expression enhances the potential universality of the ELF3-MXRA8 axis as a therapeutic target. Theoretically, therapeutic strategies targeting this axis may exert efficacy across a broader spectrum of GBM patients, regardless of their sex, age, or TP53 mutation status. Of course, this requires future validation of its robustness as a biomarker in prospective cohorts. Specifically, the TP53-independent expression pattern of this axis suggests that it may either function independently of the canonical p53 tumor suppressor pathway or lie downstream of it. This provides a potential complementary therapeutic target for TP53-mutant GBM, a subtype that is typically more aggressive and associated with limited treatment options. Furthermore, the consistent high expression of this axis across all age groups implies that it may be involved in driving the core malignant phenotypes shared by GBM in both elderly and young

patients.

Our multi-database and pan-cancer analyses further support the specificity of MXRA8 overexpression in GBM, distinguishing it from other tumor types. Interestingly, MXRA8 expression correlated significantly with MGMT, a key predictor of temozolomide response, suggesting that MXRA8 may intersect with treatment resistance pathways in GBM. Additionally, silencing MXRA8 has been shown to inhibit cell viability, proliferation, invasion, and migration, underscoring its pivotal role in sustaining the aggressive phenotype of GBM cells. These findings align with recent studies that reported MXRA8 knockdown reduces glioma cell viability and enhances chemosensitivity. Furthermore, MXRA8 has been identified as a key modulator of glioma ferroptosis and the tumor immune microenvironment[11]. However, the precise upstream signaling pathways through which MXRA8 contributes to GBM progression remain to be elucidated.

ELF3 was identified as a key transcriptional activator of MXRA8. Elevated ELF3 expression in GBM tissues correlates positively with MXRA8 levels and is associated with poor patient survival. In our study, Figure 2 provides bioinformatic predictions and expression correlation data, whereas Figures 5-6 present functional regulatory evidence derived from ChIP, dual-luciferase reporter, and rescue assays. Mechanistically, ELF3 binds directly to the MXRA8 promoter (1302–1310 bp) to activate its transcription. This functional relationship was confirmed in rescue experiments, where overexpression of MXRA8 reversed the inhibitory effects of ELF3 knockdown on GBM cell proliferation, invasion, and migration. While the rescue experiments in Figure 6 demonstrate that restoring MXRA8 expression can effectively reverse the tumor-suppressive phenotypes induced by ELF3 knockdown, it is important to

contextualize this finding within the known biology of transcription factors. We acknowledge that transcription factors like ELF3 typically regulate a repertoire of target genes, and it is unlikely that MXRA8 is its sole functional output. The purpose of the MXRA8 overexpression rescue was not to claim exclusivity but to apply a classic genetic epistasis test. A successful rescue specifically with the putative downstream target provides strong evidence that this target lies on a critical functional pathway of the upstream regulator. In this case, our data establish that the transcriptional activation of MXRA8 is a major, and functionally sufficient, mechanism through which ELF3 exerts its pro-tumorigenic effects in the studied GBM models. This does not preclude the existence of other ELF3 targets that may contribute to GBM pathogenesis in complementary or context-dependent ways. Future studies aimed at genome-wide identification of ELF3 targets in GBM will be valuable to fully delineate its transcriptional network and may reveal additional synergistic or alternative pathways.

These findings support previous research highlighting ELF3's oncogenic role in various cancers, particularly lung and ovarian cancer[16-18]. However, ELF3's involvement in GBM has not been previously documented. Interestingly, ELF3 and ELF4 share high sequence homology in the ETS DNA-binding domain, and ELF4 has been repeatedly implicated in GBM progression by preserving stem-like characteristics and regulating lipid metabolism. ELF4 is known to preserve the stem-like characteristics of GBM cells through Sox2 activation, thereby driving tumorigenesis[21]. Additionally, ELF4 serves as a key element in the microRNA-transcription factor network, linking glioblastoma receptor signaling to lipid metabolism regulation[22]. These observations suggest that ELF3, similar to ELF4, may play a multifaceted role in GBM progression, potentially acting

as a master regulator that integrates transcriptional control with downstream signaling pathways. By revealing the ELF3-MXRA8 axis, this study not only fills a critical gap in understanding ELF3's role in GBM but also underscores the therapeutic potential of targeting this regulatory network to disrupt tumor progression.

Several inconsistencies have been observed in the existing literature. In some cancers, ELF3 has been described as a tumor suppressor, underscoring the context-dependent role of this transcription factor[16, 19, 20]. Further research is necessary to identify the upstream regulators and cofactors that modulate ELF3 activity in GBM. Although the oncogenic role of MXRA8 in GBM has been emphasized, additional studies are required to better understand the biological processes downstream of MXRA8 activation.

This study has several limitations. Firstly, while the ELF3-MXRA8 axis has been validated both *in vitro* and *in vivo*, the broader signaling networks involving these proteins remain largely undefined. Secondly, the potential interactions of MXRA8 with other tumor-promoting factors or its contribution to immune modulation in the GBM microenvironment were not explored. Finally, the use of patient-derived GBM cells or organoid models could provide a more physiologically relevant system to confirm these findings and evaluate therapeutic strategies targeting the ELF3-MXRA8 axis. Future studies should aim to address these gaps by investigating the downstream signaling pathways of MXRA8 and exploring the therapeutic potential of targeting the ELF3-MXRA8 axis in combination with standard GBM therapies. Moreover, the relationship between the ELF3-MXRA8 axis and therapy resistance, as well as tumor heterogeneity, should be examined to assess its clinical relevance.

5 Conclusion

In conclusion, our study identified the ELF3-MXRA8 axis as a key driver of GBM progression. Elevated ELF3 expression activated MXRA8 transcriptionally, promoting oncogenic properties in GBM cells. These findings underscore the potential of MXRA8 as a diagnostic marker and ELF3 as a therapeutic target. By uncovering this regulatory pathway, our study offers new insights into the molecular mechanisms underpinning GBM malignancy, laying the groundwork for future research focused on developing targeted therapies to improve patient outcomes.

Authors' contributions

Maomao Wang, Haiji Bo, Dapeng Chen contributed to data curation, wrote the original draft, prepared the visualization, conducted the investigation, and validated the findings. Jiangxin Mao contributed to formal analysis, visualization, and investigation. Zong Miao and Laixing Wang oversaw project administration and reviewed and edited the manuscript. Zong Miao conceptualized the study, developed the methodology, created visualizations, and reviewed and edited the manuscript. Laixing Wang provided supervision, secured funding, and reviewed and edited the manuscript. All authors gave final approval for the manuscript.

Funding Declaration

This study was funded by the National Natural Science Foundation of China (Grant No. 82303915).

Availability of data and materials

The datasets generated and analysed during the current study are available in https://doi.org/10.7910/DVN/UFHS7Z. Additional information and resources can be obtained by contacting the corresponding authors upon request.

Human and animal rights

The study involving human participants adhered to ethical standards set by the institutional and/or research committee in accordance with the 1975 Declaration of Helsinki (revised in 2013). The animal experimental protocol followed the Guide for the Care and Use of Laboratory Animals, 8th Edition, and the study was reported in compliance with ARRIVE guidelines.

Consent for publication

All authors have consented to the publication of this manuscript.

Competing interests

The authors have no competing interests to declare.

Reference

1. Grochans, S.; Cybulska, A. M.; Siminska, D.; Korbecki, J.; Kojder, K.; Chlubek, D.; Baranowska-Bosiacka, I., Epidemiology of Glioblastoma Multiforme-Literature Review. *Cancers (Basel)* **2022,** *14* (10).

2. Roncevic, A.; Koruga, N.; Soldo Koruga, A.; Roncevic, R.; Rotim, T.; Simundic, T.; Kretic, D.; Peric, M.; Turk, T.; Stimac, D., Personalized Treatment of Glioblastoma: Current State and Future Perspective. *Biomedicines* **2023,** *11* (6).

3. Mahmoud, A. B.; Ajina, R.; Aref, S.; Darwish, M.; Alsayb, M.; Taher, M.; AlSharif, S. A.; Hashem, A. M.; Alkayyal, A. A., Advances in immunotherapy for glioblastoma multiforme. *Front Immunol* **2022,** *13*, 944452.

4. Wu, W.; Klockow, J. L.; Zhang, M.; Lafortune, F.; Chang, E.; Jin, L.; Wu, Y.; Daldrup-Link, H. E., Glioblastoma multiforme (GBM): An overview of current therapies and mechanisms of resistance. *Pharmacol Res* **2021,** *171*, 105780.

5. Al-Ghabkari, A.; Huang, B.; Park, M., Aberrant MET Receptor Tyrosine Kinase Signaling in Glioblastoma: Targeted Therapy and Future Directions. *Cells* **2024,** *13* (3).

6. Verdugo, E.; Puerto, I.; Medina, M. A., An update on the molecular biology of glioblastoma, with clinical implications and progress in its treatment. *Cancer Commun (Lond)* **2022,** *42* (11), 1083-1111.

7. Nguyen, H. M.; Guz-Montgomery, K.; Lowe, D. B.; Saha, D., Pathogenetic Features and Current Management of Glioblastoma. *Cancers (Basel)* **2021,** *13* (4).

8. Goenka, A.; Tiek, D.; Song, X.; Huang, T.; Hu, B.; Cheng, S. Y., The Many Facets of Therapy Resistance and Tumor Recurrence in Glioblastoma. *Cells* **2021,** *10* (3).

9. Simpson, K. E.; Staikos, C. A.; Watson, K. L.; Moorehead, R. A., Loss of MXRA8 Delays Mammary Tumor Development and Impairs Metastasis. *Int J Mol Sci* **2023,** *24* (18).

10. Zhang, R.; Kim, A. S.; Fox, J. M.; Nair, S.; Basore, K.; Klimstra, W. B.; Rimkunas, R.; Fong, R. H.; Lin, H.; Poddar, S.; Crowe, J. E., Jr.; Doranz, B. J.; Fremont, D. H.; Diamond, M. S., Mxra8 is a receptor for multiple arthritogenic alphaviruses. *Nature* **2018,** *557* (7706), 570-574.

11. Xu, Z.; Chen, X.; Song, L.; Yuan, F.; Yan, Y., Matrix Remodeling-Associated Protein 8 as a Novel Indicator Contributing to Glioma Immune Response by Regulating Ferroptosis. *Front Immunol* **2022,** *13*, 834595.

12. Tan, L.; Fu, D.; Liu, F.; Liu, J.; Zhang, Y.; Li, X.; Gao, J.; Tao, K.; Wang, G.; Wang, L.; Wang, Z., MXRA8 is an immune-relative prognostic biomarker associated with metastasis and CD8(+) T cell infiltration in colorectal cancer. *Front Oncol* **2022,** *12*, 1094612.

13. Simpson, K. E.; Watson, K. L.; Moorehead, R. A., Elevated Expression of miR-200c/141 in MDA-MB-231 Cells Suppresses MXRA8 Levels and Impairs Breast Cancer Growth and Metastasis In

Vivo. *Genes (Basel)* **2022,** *13* (4).

14. Ichihara, R.; Shiraki, Y.; Mizutani, Y.; Iida, T.; Miyai, Y.; Esaki, N.; Kato, A.; Mii, S.; Ando, R.; Hayashi, M.; Takami, H.; Fujii, T.; Takahashi, M.; Enomoto, A., Matrix remodeling-associated protein 8 is a marker of a subset of cancer-associated fibroblasts in pancreatic cancer. *Pathol Int* **2022,** *72* (3), 161-175.

15. Song, D.; Jia, X.; Liu, X.; Hu, L.; Lin, K.; Xiao, T.; Qiao, Y.; Zhang, J.; Dan, J.; Wong, C.; Hu, C.; Sai, K.; Gong, S.; Sander, M.; Shen, R.; Chen, X.; Xiao, X.; Chen, J.; Zhang, Y.; Wei, C.; Xiao, X.; Liang, J.; Zhang, Q.; Hu, J.; Zhu, W.; Yan, G.; Lin, Y.; Cai, J., Identification of the receptor of oncolytic virus M1 as a therapeutic predictor for multiple solid tumors. *Signal Transduct Target Ther* **2022,** *7* (1), 100.

16. Ju, Y.; Fang, S.; Liu, L.; Ma, H.; Zheng, L., The function of the ELF3 gene and its mechanism in cancers. *Life Sci* **2024,** *346*, 122637.

17. Kuang, L.; Li, L., E74-like factor 3 suppresses microRNA-485-5p transcription to trigger growth and metastasis of ovarian cancer cells with the involvement of CLDN4/Wnt/beta-catenin axis. *Saudi J Biol Sci* **2021**, *28* (8), 4137-4146.

18. Liu, Y.; Wang, S.; Zhou, R.; Li, W.; Zhang, G., Overexpression of E74-like transformation-specific transcription factor 3 promotes cellular proliferation and predicts poor prognosis in ovarian cancer. *Oncol Lett* **2021,** *22* (4), 710.

19. Suzuki, M.; Saito-Adachi, M.; Arai, Y.; Fujiwara, Y.; Takai, E.; Shibata, S.; Seki, M.; Rokutan, H.; Maeda, D.; Horie, M.; Suzuki, Y.; Shibata, T.; Kiyono, T.; Yachida, S., E74-Like Factor 3 Is a Key Regulator of Epithelial Integrity and Immune Response Genes in Biliary Tract Cancer. *Cancer Res* **2021,** *81* (2), 489-500.

20. Gondkar, K.; Patel, K.; Krishnappa, S.; Patil, A.; Nair, B.; Sundaram, G. M.; Zea, T. T.; Kumar, P., E74 like ETS transcription

factor 3 (ELF3) is a negative regulator of epithelial- mesenchymal transition in bladder carcinoma. *Cancer Biomark* **2019,** *25* (2), 223-232.

21. Bazzoli, E.; Pulvirenti, T.; Oberstadt, M. C.; Perna, F.; Wee, B.; Schultz, N.; Huse, J. T.; Fomchenko, E. I.; Voza, F.; Tabar, V.; Brennan, C. W.; DeAngelis, L. M.; Nimer, S. D.; Holland, E. C.; Squatrito, M., MEF promotes stemness in the pathogenesis of gliomas. *Cell Stem Cell* **2012,** *11* (6), 836-44.

22. Kosti, A.; Chiou, J.; Guardia, G. D. A.; Lei, X.; Balinda, H.; Landry, T.; Lu, X.; Qiao, M.; Gilbert, A.; Brenner, A.; Galante, P. A. F.; Tiziani, S.; Penalva, L. O. F., ELF4 is a critical component of a miRNA-transcription factor network and is a bridge regulator of glioblastoma receptor signaling and lipid dynamics. *Neuro Oncol* **2023,** *25* (3), 459-470.